Adsorption kinetics of acetic acid into ZnO/castor oil-derived polyurethanes

Adsorption kinetics of acetic acid into ZnO/castor oil-derived polyurethanes

Alessio Zuliani,[a] David Chelazzi,[a]* Rosangela Mastrangelo,[a] Rodorico Giorgi,[a] Piero Baglioni[a]*

[a]Department of Chemistry "Ugo Schiff" and CSGI, University of Florence, Via della Lastruccia 3, 50019 Sesto Fiorentino, Florence, Italy

Corresponding Authors

*E-mail: piero.baglioni@unifi.it; david.chelazzi@unifi.it Phone: +390554573033; +390554573049

Abstract

Hypothesis

Materials and colloids science can provide significant contributions to the conservation of Cultural Heritage. Hybrid systems made of a castor oil-derived polymeric network and a disperse phase of zinc oxide particles (ZnO/COPs) can be more effective absorbers of acetic acid (AcOH, a major pollutant harmful to artifacts in museums and art collections) than state-of-the-art materials, provided the acid uptake mechanism by the hybrids is elucidated and optimized. The starting hypothesis was that the polymer matrix might act as transporter, while acid adsorption would take place at the ZnO particles surface. The effect of particles size was expected to play a significant role.

Experiments

The adsorption kinetics of the hybrids were studied in the 23-45˚C range, in comparison with activated charcoal, the benchmark employed by conservators. Morphological and fractal dimension of ZnO micro- and nano-particles in the hybrid networks were investigated and correlated to the adsorption kinetics.

Findings

The presence of a two-steps mechanism for AcOH uptake by the hybrids was demonstrated for the first time, a combination of Fickian diffusion and Case-II transport occurs in the COP matrix, and adsorption dominates acid uptake (followed by neutralization) at the particles surface. This mechanism is likely key to explain the enhanced performances of the hybrids vs. activated charcoal and state-of-the-art tools to remove AcOH. The hybrids have high uptake capacity, and lower activation energies for the removal process than materials where the uptake of acid relies solely on adsorption. The size of the ZnO particles contributes to the process, i.e. nanoparticles form smaller and ramified fractal clusters that are able to adsorb AcOH more effectively than microparticles. These insights demonstrated the efficacy of the novel hybrids in art conservation, where the control of minimal concentrations of VOCs is crucial for the preventive conservation of masterpieces, and can be useful to other fields where efficient capture of acetic acid is critical (food industry, textile dyeing/printing, *etc*.).

Keywords

Abbreviations

ZnO, zinc oxide; VOC, volatile organic compounds; AcOH, acetic acid; PolyHDI, poly(hexamethylene diisocyanate); COP, castor oil polyurethane; HCPs, hypercrosslinked polymers; GC, gas chromatography; PFO, pseudo-first order; PSO, pseudo-second order; DE, double exponential; SRT statistical rate theory; $\chi 2$, chi square; ARE, average relative error; SSE, sum of the squares of the errors; EABS, sum of the absolute errors; HYBRID, composite fractional error function; MPSD, Marquand's percent standard deviation; Rs, gyration radius; ξ, correlation length; S, weighted average of the areas of the clusters; D, Hausdorff fractal dimension; Ea, activation energy.

Adsorption, Kinetics, Polyurethanes, Castor oil, Acetic acid, Zinc oxide, Zinc acetate, VOCs removal, Preventive conservation, Cultural Heritage conservation

1. Introduction

The preservation of Cultural Heritage has fundamental socio-economic impacts, since well-conserved and accessible historical/artistic assets drive the creation of jobs (*e.g.*, through tourism) and the improvement of life quality in the citizens' communities. Conservation challenges involve preventive and remedial measures aimed at counteracting the degradation of works of art caused by environmental factors such as light, temperature, relative humidity, pollutants, microorganisms, and even by anthropic causes like vandalism or wrong restoration interventions. In this framework, colloids, material science and soft matter have been contributing in the last decades effective materials and methodologies for the remedial conservation (*i.e.*, restoration) of artifacts spanning from ancient objects to the classic, modern and contemporary production.[1-5] In addition, colloidal systems and advanced materials can prove highly beneficial also in preventive conservation, in particular in pollution remediation, *i.e.*, the removal of detrimental volatile organic compounds (VOCs) and other degradation agents, from museum display cases, archive boxes and storage crates.[6-7] In particular, while synthetic and bio-polymers are being explored in the formulation of hydrogels and organogels for the cleaning of works of art,[8-12] their use for pollution remediation in art conservation is still in its infancy and there is large room for the development of innovative materials.

Inspired by national and international environmental policies and recent trends in the development of green and sustainable materials,[13-19] we proposed a new environmentally friendly hybrid (organic–inorganic) hypercrosslinked resin for the removal of acetic acid (AcOH). AcOH is a major VOC pollutant present in museum enclosures and collections, which need to be efficiently removed to avoid damage to the artifacts.[7] Essentially, a

sustainable biomass-derived hypercrosslinked polyurethane made of castor oil and poly(hexamethylene diisocyanate) (PolyHDI) was used to create a hybrid composite material where ZnO micro- or nanoparticles are confined and used to remove AcOH through the formation of zinc acetate. A synergistic effect was demonstrated between the polymer network and the dispersed particles in the zinc oxide-castor oil polyurethane hybrids (ZnO/COPs): AcOH is captured through weak interactions with the polyurethane and transported inside the network up to the surface of the ZnO particles, where the acid is neutralized into (zinc) acetate. However, the mechanism of AcOH uptake by the ZnO/COPs was not elucidated, and the high number of possible combinations in the absorbing hybrids, *e.g.*, in terms of ZnO content, size and surface area of the particles, demands for a quantitative investigation protocol. Namely, the effect of different components on the performance of the systems must be evaluated, so as to boost their systematic optimization. The new hybrid absorbers proposed here, aim at providing a significant step forward in pollution remediation, overcoming the limitations of several state-of-the-art absorbers. Namely: i) metal-organic frameworks (MOFs) can have high VOC uptake capability, but also exhibit high manufacturing costs;[20] ii) natural porous materials (activated carbons, zeolites) have affordable manufacturing costs and environmentally friendly characteristics, but adsorb VOCs mainly via physisorption, and can thus release them in large amounts following temperature fluctuations, turning into VOCs sources;[21, 22] in addition, they can show deliquescence or surface crystallization of acetate salts,[23] likely due to their high Henry constants; iii) hypercrosslinked polymeric resins are relatively inexpensive and have good VOCs adsorption capacities, but are typically petroleum-based and thus less environmentally sustainable.[24, 25]

Being based on the combination of a biomass-derived resin matrix and inorganic particles able to stably neutralize AcOH, the new ZnO/COPs are expected to work on a multiple-step

uptake process and can avoid the aforementioned limitations, surpassing state-of-the-art VOC absorbers, provided their AcOH uptake mechanism is fully understood and optimized. Here, quantitative information is provided for the first-time on the kinetics of absorption of AcOH in the ZnO/COPs. The AcOH uptake into the ZnO/COPs was studied using different models, including diffusion-controlled, double-exponential, transport, and adsorption-controlled kinetics, in comparison with activated charcoal, the benchmark employed by conservators. The VOC uptake was measured for systems by varying the ZnO content and the dimensions of the particles, operating at different working temperatures in the 23-45˚C range to evaluate the activation energies for the absorption process.

In addition to its purpose in art conservation, this study also aims at providing further insight in the absorption mechanisms of hypercrosslinked polymers (HCPs), a class of materials with a wide range of transversal applications from gas sorption/separation, to drug delivery, catalysis, cosmetics, and chromatography.[26-28] The literature comprises several studies on the removal of contaminants by HCPs from aqueous solutions,[29-35] and for the gas-phase removal of some VOCs, including benzene, dichloromethane, some ketones and esters.[36-41] However, the use of hybrid organic-inorganic HCPs as VOCs absorbers is, to the best of our knowledge, still largely unexplored, in particular for the removal of AcOH. This is of high interest considering that the acid is employed in many industrial manufacturing processes as well as in food industry and textile dyeing or printing, and is known to exhibit some toxicity, with a mild irritative effect already at a few ppm concentration.[42, 43]

2. Materials and Methods

2.1 Materials

Castor oil (Pharma grade, 89.2%$_{wt}$ of ricinoleic acid) was purchased from Gioma Varo Srl (Milan, Italy). Poly(hexamethylene diisocyanate) (polyHDI, 1,300-2,200 cP), ZnO powder (<5 μm particle

size, 99.7 % calculated on calcined substance), ethanol (absolute, reag. ISO, reag. Ph. Eur., ≥99.8% (GC)), and acetic acid (AcOH) (glacial, ReagentPlus®, ≥99%) were purchased form Sigma Aldrich (Milan, Italy). ZnO nanopowder (20 nm average particles size, >99% trace metals basis) was purchased from Ionic Liquids Technologies GmbH (Heilbronn, Germany). Commercially available (for industrial purposes) ZnO powder (<44 μm particle size, >99.9%, Pharama grade) was purchased from L'Aprochimidie Srl (Muggiò, Italy). Activated charcoal (Activated Charcoal K48, from coconut shells) was purchased from Long Life for Art GmbH (Eichstetten, Germany). All reagents were used without any further purification. ZnO powders were dried at 120°C during 48 hours before utilization, to remove all eventually adsorbed moisture.

2.2 Synthesis of the ZnO/COPs

The ZnO/COPs samples were prepared according to a recently reported procedure.[7] Specifically, castor oil and the crosslinking agent, poly(hexamethylene)diisocyanate (PolyHDI), were firstly vigorously stirred for 15' at room temperature. Sequentially, the selected type (<5 μm particle size, <44 μm particle size and 20 nm average particles size) and amount (10, 30 or 60%$_{wt}$) of ZnO powder was added and mixed for other 15' at room temperature. Lastly, the mixture was poured into 3.5 cm diameter x 0.4 cm height silicone molds and cured in oven at 90 °C. ZnO/COPs were removed from the molds and directly employed for the kinetic studies of absorption of AcOH.

2.3 VOCs adsorption tests

Adsorption curves were determined by gravimetric analysis plotting adsorption capacities, *i.e.*, mass (g) of AcOH adsorbed *per* mass (g) of material, in function of time (h). In each experiment, the selected ZnO/COP sample, in the form of a disk of *ca.* 4 g, 3.60 cm diameter and 0.44 cm height, and a 10 mL vial filled with 8 mL AcOH were closed and sealed in a 200 mL glass round bottle

equipped with a screw cap, and placed in a thermal chamber at 23, 35, 40 and 45 ±0.3°C. In this way, a saturated atmosphere of AcOH was produced inside the bottle. The ZnO/COP cylinder was weighted at regular time. Likewise, *ca.* 4 g of pure ZnO powders, or activated charcoal (used as benchmark), were placed in glass vials of the same dimension of the ZnO/COPs cylinders, and their adsorption capacities were studied in the same way as for the ZnO/COPs.

2.4 Characterization techniques

SEM images of ZnO/COP samples 30%44µm, 30%5µm and 30%nano were recorded with a FEG-SEM Gemini scanning microscope (Carl Zeiss Microscopy, Germany), working at 30 kV at a working distance of 4.5 mm.

Five SEM images for each sample were cut in 2004x2004 pixels images and binarized through MATLAB built-in functions. The images were then analyzed through a MATLAB routine adapted from Frydendahl *et al*.[44], which allowed the identification of particles clusters (2D objects constituted by white pixels, with a 8-point connectivity). Geometrical parameters describing clusters where calculated through the routine: the perimeter *vs.* area relationship for each aggregate, the gyration radius, Rs, the correlation length, ξ, the weighted average of the areas of the clusters, S, and the Hausdorff fractal dimension, D. The cumulative results and further details about the calculations are reported in the Results and Discussion section.

A Renishaw InvIa Qontor confocal MicroRaman was used to acquire Raman spectra and 2D mapping on ZnO/COP samples 30%44µm and 30%nano, before and after the interaction with AcOH. The confocal MicroRaman is equipped with a solid-state laser (785 nm, IPS R-type NIR785, 200 mW, 1200 l/mm grating), a front-illuminated CCD camera (655 × 1024 px, working temperature −70°C) and a research-grade Leica DM 2700 microscope. A 100X L (long working) objective was used, with a laser power of 20mW, and a spot size of 1.27 µm.

Single spectra were recorded in the 100 to 3200 cm^{-1} range (extended range mode). A range of interest was identified for ZnO micro- and nanoparticles (380 – 1530 cm^{-1}) and for zinc acetate

crystals (212 – 1400 cm^{-1}), to map their characteristic signals in 2D Raman maps. Maps of 14 x 20 μm^2 were acquired, with steps of 1 μm. Raw data were processed with the Renishaw software WiRE v.5.2, and false-color maps were generated, showing the abundance of ZnO micro- and nanoparticles in on ZnO/COP samples 30%44μm and 30%nano, and zinc acetate crystals in the same samples after exposure to AcOH.

3. Results and discussion

3.1 Characteristics of the ZnO/COPs and possible adsorption kinetic models

As schematically illustrated in Fig.1, the ZnO/COPs are hybrid organic-inorganic hybrids where ZnO particles are dispersed in a continuous phase of a polyurethane network. Such hybrid structure allows preparing flexible films for the removal of AcOH alternative to commonly employed activated charcoal, a powder difficult to handle and use (*e.g.*, it can be spread over a masterpiece, damaging it).

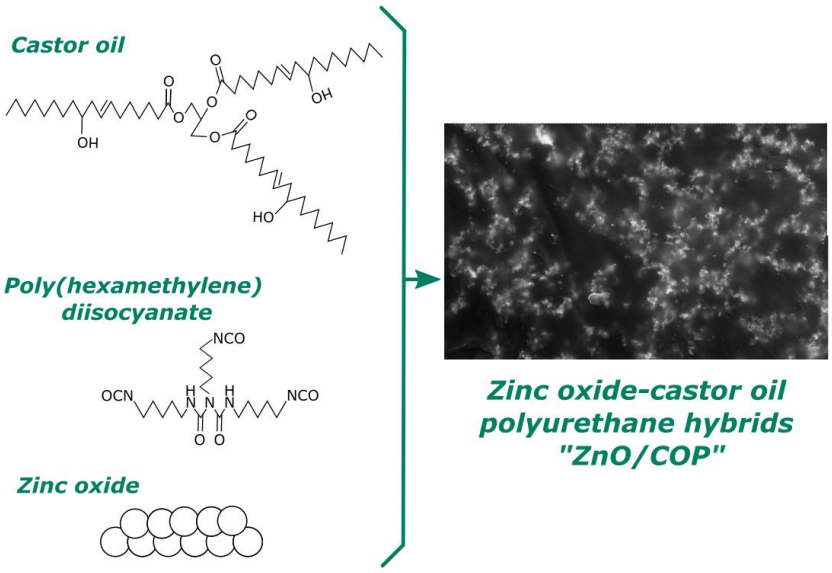

Fig. 1. Scheme of the preparation of the ZnO/COPs sample, yielding a polymeric network where ZnO particles are embedded (as evidenced by the SEM image of the hybrid section, see next sections for details).

The adsorption capacities of COP and ZnO/COPs for the removal of AcOH were evaluated as a function of the exposure time and at different temperatures, ranging from 23 to 45°C, in the saturated AcOH atmosphere. As a reference, the adsorption capacities of pure ZnO powders and commercially available activated carbon were also determined. In general, adsorption curves were measured until equilibrium was reached in the acid uptake by the sorbents. In some cases, however, the sorbents started to degrade before reaching the equilibrium, due to the strong acidic conditions, *e.g.*, liquescence was observed on the surface of the resins, or ZnO/zinc acetate grains were disaggregated by extensive exposure/sorption. Such degradation of the sorbents can cause oscillations or deviations in the uptake curves that introduce large errors in the fitting of the curves at high exposure time.

Table 1. ZnO/COPs samples and ZnO powders used for the adsorption tests.

Sample name	**Sample type**	**Type of ZnO**	**ZnO %$_{wt}$**
COP	COP resin	/	0
10%nano	ZnO/COP hybrid	20 nm average particles size	10
30%nano	ZnO/COP hybrid		30
60%nano	ZnO/COP hybrid		60
10%5µm	ZnO/COP hybrid	<5 µm particle size	10
30%5µm	ZnO/COP hybrid		30
60%5µm	ZnO/COP hybrid		60
10%44µm	ZnO/COP hybrid	<44 µm particles for industrial purposes	10
30%44µm	ZnO/COP hybrid		30
60%4µm	ZnO/COP hybrid		60
ZnO-nano	ZnO powder	20 nm average particles size	100
ZnO-5µm	ZnO powder	<5 µm particle size	100
ZnO-44µm	ZnO powder	<44 µm, particles for industrial purposes	100

The composition of the ZnO/COPs samples used in this study (see Table 1) had been previously characterized by means of infrared spectroscopy, thermogravimetric analysis, and scanning electron microscopy, before and after the adsorption tests.[7] It is useful to recall here some of the structural features of the pure and hybrid COP networks, since this information can be helpful in the interpretation of the AcOH uptake kinetic data.

First, while the pure COP has a compact morphology at the micron-scale, the ZnO/COPs hybrids exhibit bubble-like cavities of 10-350 μm across their volume. These cavities likely form when CO_2 is produced by the reaction of isocyanate with water residues dissolved in castor oil; such reaction is favored by the presence of ZnO that acts as catalyst for the nucleophilic attack of hydroxyls to isocyanate.[7] The ZnO particles are found through the section and in the pores of the polyurethane network. The conversion of ZnO into zinc acetate was observed by FTIR 2D Imaging in previously reported work;[7] in particular IR absorption peaks at 1595 and 1542, 1430 and 1380 cm^{-1} were detected in the ZnO/COPs hybrids after their interaction with AcOH, and corresponded to, respectively, the zinc acetate COO^- asymmetric and symmetric stretching vibrations, and CH_3 symmetric bending. In addition, mapping the intensity of the 1595 cm^{-1} peak clearly showed the presence of zinc acetate domains all over the surface and through the bulk of the composite; the domains' dimensions (10-500 μm) match those of the crystals showed by SEM in the acid-exposed composites [7]. Overall, this clearly indicated that AcOH, transported through the COP matrix, is able to interact with the ZnO particles, which neutralize the acid.

The interaction between the composites and AcOH was further studied and analyzed here by confocal Raman measurements. The E_2 optical phonon band of ZnO [45, 46] (438 cm^{-1}, Fig. S1A, B in the Supporting Information) allowed tracing the clusters formed in the 30%44μm and 30%nano ZnO/COP samples. The C-C stretching of acetate [47] (~954 cm^{-1}, Fig. S1C in the Supporting Information), instead, was used to evidence the shape of zinc acetate crystals, formed after the exposure of both samples to AcOH. The false-color 2D maps (Fig. 2 and Fig. S2-S3 in the Supporting Information) show that ZnO micro- and nanoparticles form micron-sized clusters that

are homogeneously distributed in the COP matrix; Raman bands associated to the COP matrix are clearly identifiable: the C-O and C-C polarization in the 850-870 cm^{-1} range, and the O=C-O stretching of the ester group at 1303 cm^{-1} indicate the presence of castor oil,[48, 49] while the band around 1250 cm^{-1} can be related to the urethane amide [50] (Fig. 2A and Fig. S2). The formation of Zinc Acetate crystals, on the other hand, leads to the observation of specific Raman bands that completely cover absorptions from the matrix, even in the optical image background: bands at 315 and 520 cm^{-1} have been reported for anhydrous $ZnAc_2$,[51] while at 1355 cm^{-1} the acetate CH_3 stretching can be observed.

The size and fractal dimension of these clusters is expected to significantly affect the AcOH uptake kinetics of the hybrids, and this issue was investigated thoroughly in this contribution (see sections 3.4 and 3.5). After the exposure of the samples to AcOH, the clusters merge and form zinc acetate crystals of tens of microns, see the Supporting Information for some additional images and discussion.

The ZnO/COPs retain high amounts of AcOH even after desorption (*i.e.*, by placing the ZnO/COPs outside the saturated atmosphere of AcOH), as they stably transform the acid into (zinc) acetate. Instead, the pure COPs retain very low amounts, suggesting that the polyurethane network interacts with the VOC through weak physisorption. In principle, one might expect thus a larger contribution of diffusion in the absorption mechanism of the pure COP, and a more significant contribution of adsorption-controlled processes in the hybrids. In addition, there was the need to verify the hypothesis that weak polyurethane-AcOH interactions are responsible for boosting the absorption capability of the Zn/COPs in a synergistic effect: the acid is taken up by the polyurethane network, and then is neutralized at the surface of the ZnO particles all across the volume of the resin.[7] Therefore, transport mechanisms are expected to play a significant role in the description of the uptake process.

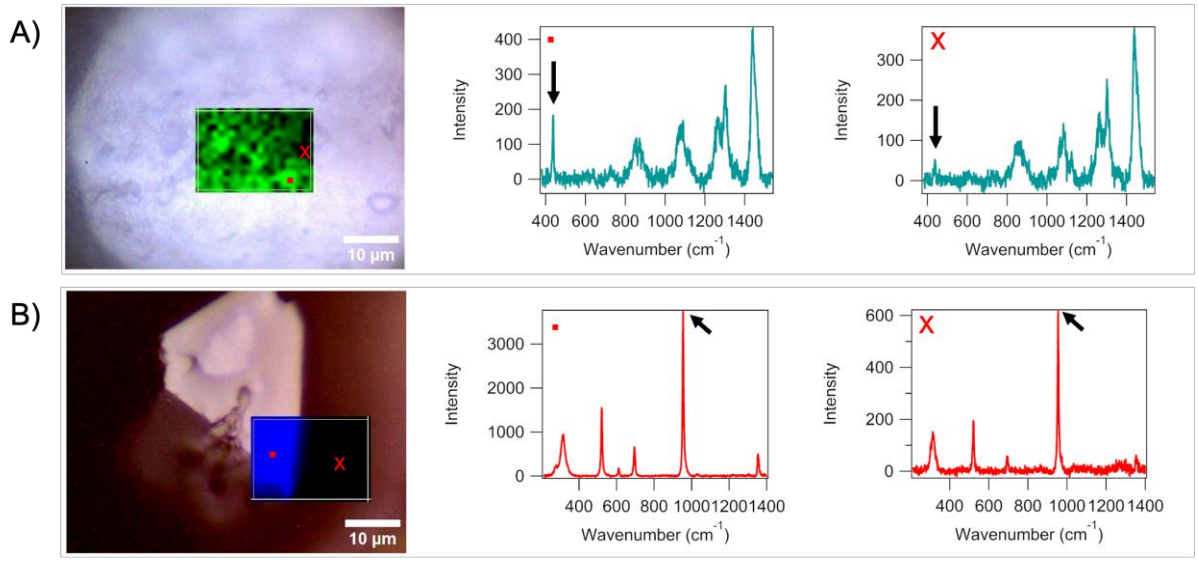

Fig. 2. A) Left: false color maps obtained tracking the 438 cm^{-1} peak of ZnO on the 30%nano ZnO/COP, before exposure to AcOH, showing the abundance of ZnO clusters (green) in the sample. Right: Raman spectra related to green (ZnO clusters) or black pixels (COP background) in the false color maps. B) Left: false color maps obtained tracking the ~954 cm^{-1} peak of acetate on the 30%nano ZnO/COP (bottom), after 1500 h exposure to AcOH, showing crystals of zinc acetate in the samples. Right: Raman spectra related to blue (zinc acetate crystals) or black pixels (ZnO/COP background) in the false color maps. The spectra and false color maps relate to depths of 5-30 µm from the surface of the samples.

While these considerations make some reasonable physical sense, they are not completely exhaustive in guiding the *a priori* selection of a specific sorption kinetic model, among those proposed in the literature, to fit the experimental uptake curves. In fact, linking mathematical kinetic models to actual physico-chemical mechanisms in the overall sorption process is still the object of dedicated studies.[52-54] It is useful to report here a concise rationale behind the different models currently adopted in the literature, before critically applying some of them to the uptake of AcOH by the ZnO/COPs.

Sorption processes are generally schematized with a series of three consecutive steps that include the solute transport in the bulk solution and its diffusion in liquid films at the surface of the sorbent particles (for solid/solution systems) (I), diffusion of the solute in the pores and along the pore walls of the particles (II), and adsorption/desorption of the solute on/from the surface of the particles surface (III) [53-55]. The overall rate of the sorption process can be controlled by one of the steps, or their combination.

Diffusion-controlled models typically include intraparticle diffusion (IPD),[56, 57] diffusion-adsorption,[58] adsorption dynamic intraparticle model,[59] and double exponential.[60] In particular, IPD is the most popular reported in the literature to describe sorption processes entirely controlled by diffusion, thus it was selected to determine if the diffusion was indeed the only main limiting-step in the AcOH uptake by the pure COP system. The diffusion-adsorption model proposed by Simonin [58] can account for a mixed process, and holds when solute concentration is high, but requires knowing the solute diffusion coefficient in the adsorbent, which is generally difficult to measure experimentally and was not available at this stage. This model converges to classical IPD for short diffusion times. Pore and surface diffusivities of the particles and a film mass transfer parameter, required in the adsorption dynamic intraparticle model proposed by Russo *et al.*,[59] were also hardly accessible, hindering good correlation between data fits and directly measured values. Fitting of the uptake curves with double exponentials was carried out to investigate the presence of a two-step mechanism in the AcOH sorption by the COP and ZnO/COPs.

Regarding adsorption-controlled kinetic models, the focus was on Pseud-first order (PFO), pseudo-second order (PSO), and Elovich models, which are among the most popular kinetic equations reported in the literature.[54] Their success mainly derives from the use of simple equations that are able to produce good fits of experimental data for the sorption of different kinds of solutes by various sorbents. Even if they were introduced as essentially empirical models, PFO and PSO were considered as order-based since it is generally argued that they relate to, respectively,

a one-site (PFO) or two-site (PSO) occupancy adsorption by the adsorbing molecule on the sorbent surface. However, because appropriate models should in principle be based on a rigorous approach to interfacial kinetic processes, some authors have provided theoretical background to derive the PFO and PSO equations as approximate solutions of fundamental models, such as that originally proposed by Langmuir or the more recent Statistical Rate Theory (SRT) approach to the transport of molecules between two neighboring phases.[52, 53] The Elovich equation, theoretically connected with strongly heterogeneous sorbent surfaces [61, 62], is considered to be applicable mainly to the initial phases of the sorption process, as it neglects the rate of simultaneously occurring desorption.[53]

Finally, to account for transport mechanisms it was decided to fit the uptake curves with the Weibull function,[63] an empirical formula typically employed in the analysis of dissolution and release studies, to determine whether a process is governed by Fickian transport (*i.e.*, diffusion), a combination of Fickian diffusion and Case-II transport, or complex transport mechanisms.

The detailed equations for the kinetic models used to fit the uptake curves are reported in the Supporting Information. The fitting equations were used on the original scale ($y = q(t)$, where q is the amount of adsorbed solute *per* grams of sorbent) rather than transformed scales or linearized forms, to obtain statistically relevant comparisons, *i.e.*, understand which model provides better fits.[54, 64] The fitting of the experimental adsorption data to the models was evaluated through different non-linear error functions including Chi Square ($\chi 2$), Average Relative Error (ARE), Sum of the Squares of the Errors (SSE), Sum of the Absolute Errors (EABS), Composite Fractional Error Function (HYBRID) and Marquand's Percent Standard Deviation (MPSD).[65]

3.2 Adsorption kinetics of hypercrosslinked polymer COP: effect of temperature

The kinetic study initially focused on the AcOH adsorption by the mere hypercrosslinked polymer COP, *i.e.*, the castor oil-derived polyurethane without the ZnO particles, whose understanding served as a basis before investigating the hybrid systems.

Overall, no satisfactory fittings could be obtained with the Elovich and IPD models, while PFO, PSO, Weibull and DE showed lower fitting errors; in all cases, PSO gave significantly better fits than PFO (see Fig. S4-6 and Annex I in the Supporting Information for the complete fitting data for the COP samples). In particular, at 23°C, the Weibull model provides the best fit, even slightly better than PSO, as confirmed by comparing the different non-linear error values for the two fits.

At 23°C, the n_w value given by the Weibull fit is 0.76±0.01, close to the limit between pure Fickian diffusion ($n_w \leq 0.75$) and a combination of Fickian diffusion and Case-II transport ($0.75 < n_w < 1$). Overall, this indicates that, at that temperature, the uptake of AcOH into the COP is mainly controlled by diffusion through the polyurethane network (good fit with Weibull), and partly by weak interactions (physisorption) between the network and AcOH (slightly worst fit with PSO).

Increasing the temperature, however, resulted in PSO providing a significantly better fit than the Weibull model. This is likely due to faster diffusion at higher temperature, while competition between thermal energy and weak COP-AcOH interactions makes the latter less and less favorable, *i.e.*, the acid uptake becomes more adsorption-limited.

In all cases, the DE model gives good fits of the experimental data, confirming the presence of a two-steps uptake process.

3.3 Adsorption of the 30%44µm Zn/COP: comparison with ZnO powders and activated charcoal

In the previous evaluation of the AcOH adsorption by the ZnO/COPs, the 30%44µm hybrid system was selected as the ideal candidate for end-users and production upscale, since it combines good

adsorption capacity (*ca.* 0.45 g AcOH *per* g of hybrid resin, after more than 1500 h adsorption followed by desorption cycles) with reduced production costs and optimal mechanical properties [7] (Fig. 3A-D). Overall, it is versatile and suitable for different applications, such as solid sponge in a display case (Fig. 3E) or as protective foil on the back of a painting inside a frame (Fig. 3F)

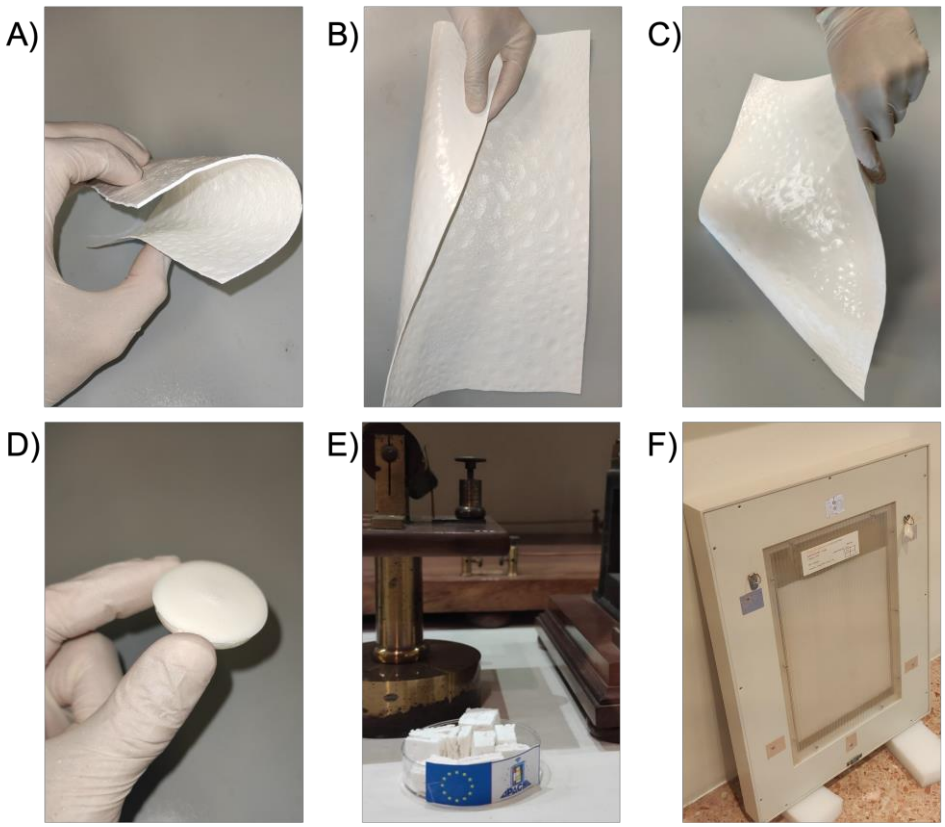

Fig. 3. The panels show how 30%44µm ZnO/COPs can be prepared in different shapes and are easily handled and bent (A-D) to adapt to applications in various types of museum settings such as solid sponges in display cases (E), and foils included in the backside of a painting frame (F).

Increasing the ZnO content up to 60%$_{wt}$ almost doubles the adsorption capacity, but makes the hybrids crumbling, which can hinder their handling by end-users and cause potential contamination of works of art when these systems are employed inside display cases or storage crates. Even though they have smaller surface areas, the micron-sized ZnO particles in the resins gave comparably good adsorption capacity than their nano-sized analogue, which was explained

considering some aggregation of the nanoparticles occurring during the preparation steps of the 10%nano, 30%nano and 60%nano hybrids.[7] Clustering of the particles was further confirmed by SEM image analysis, as detailed in Section 3.5. In view of these aspects, this section reports on the AcOH uptake of the 30%44µm, 30%5µm and 30%nano Zn/COP systems over time, to validate in detail their adsorption capability in comparison with the ZnO powders and the activated charcoal benchmark simply packed in vials. We decided to focus here only on the uptake comparison, leaving the fitting of the uptake curves to the following sections.

The uptake capabilities are compared at 23°C, that is close to the operative temperature found in most of the enclosures in art exhibitions, including museums and art galleries.

As showed in Fig. 4 and in Fig. S7-8 in the Supporting Information, all the ZnO/COPs and ZnO powders adsorbed more AcOH than activated charcoal.

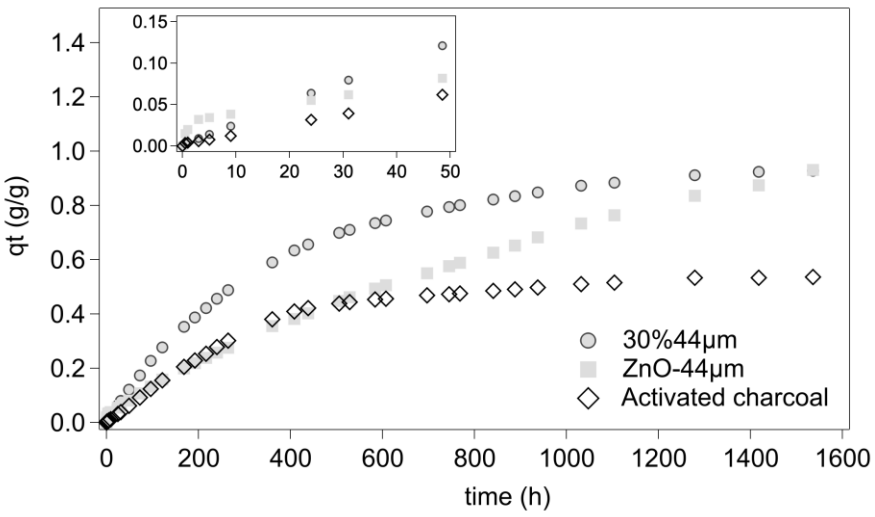

Fig. 4. Adsorption of AcOH by ZnO/COP sample 30%44µm, ZnO-44µm powder and the activated charcoal benchmark, in saturated atmosphere of AcOH at 23°C. The inset details the first 50 h of the uptake process. Errors on the experimental data are included in the markers.

This holds even when the charcoal powder is distributed loosely on the bottom of the AcOH-containing bottle, rather than packed in a vial, maximizing its exposed surface (see Fig. S9 in the Supporting Information). After initial rapid adsorption of the acid, the charcoal powder equilibrated at *ca.* 0.5 g of AcOH *per* g of sorbent, in agreement with the data reported in the literature.[66] Despite this fast initial adsorption, powdery activated charcoal has some disadvantages that make it not suitable for many practical applications in cultural heritage preservation. Firstly, loose powders can pose health risks to operators. In addition, loose powdery residues might contaminate works of art when the powders are used in frames or cases, in close contact with or near the artifacts. Lastly, the charcoal gives physical interactions with AcOH, rather than chemical bonds, as opposed to acid neutralization by the ZnO particles; thus, depending on environmental conditions, activated charcoal can release the adsorbed AcOH.[7]

By comparing the Zn/COPs (30%$_{wt}$ ZnO content) with the corresponding ZnO powders (Fig. 4 and Fig. S7-8 in the Supporting Information), it can be noticed that the hybrid systems initially adsorbed more AcOH, while after some days the powders exhibit higher uptake. Specifically, the smaller the particles, the earlier the crossover of the uptake curves occurred, *i.e.*, passing from *ca.* 1540 h to *ca.* 1280 h and 700 h respectively for systems with ZnO-44μm-, ZnO-5μm- and ZnO-nano powders. The uptake curves of the ZnO powders become steeper at *ca.* 800 h and *ca.* 550 h for, respectively, the micro- and nano-sized particles, corresponding to the point in the uptake process where the grains of the powders started to disaggregate by extensive exposure/sorption. This arguably increased the surface area available for taking up AcOH.

It was also observed that, even though the ZnO/COPs 30%44μm, 30%5μm and 30%nano have close values of maximum adsorption capacity, their uptake curves exhibit different profiles, in particular when nanosized ZnO particles are included in the COP (see also Fig. S10 in the Supporting Information). Such behavior was further analyzed by fitting the curves to different kinetic models, as detailed in the following sections.

3.4 Adsorption kinetics of the ZnO/COPs: effect of the content and dimension of the ZnO particles

As a general feature, the AcOH uptake curves of the ZnO/COPs were better fitted by PFO or PSO, rather than IPD or Weibull models, regardless the dimension/content of the ZnO particles, and over the whole investigated temperature range (23-40˚C). ZnO particles thus play a role in the kinetics of AcOH adsorption, as shown in Annex 1, SI. However, as later recalled by Simonin,[54] there are studies in the literature where PFO/PSO provided good fitting of the experimental data even though diffusion was found to significantly contribute to the process. In the case of the ZnO/COPs, the presence of two steps in the AcOH uptake was confirmed by the good fittings obtained with the DE model. In general, IPD did not fit the uptake curves well, while better fittings were obtained with the Weibull model, with values of the n_w parameter comprised between 0.75 and 1. Overall, this indicates that the transport of AcOH through the polyurethane network contributes to the rate-controlling step, through a combination of Fickian diffusion and Case-II transport, along with the adsorption of the acid at the surface of the ZnO particles.The divergence between PFO/PSO and the Weibull model decreases when smaller ZnO particles are included in the hybrid sorbents (see Fig. S11 and S12). This can be reasonably explained considering that reducing the size of the particles increases their surface area and the number of sites available for adsorption, making the diffusion and transport steps more relevant in the overall uptake process.

Fig. 5-6 show another relevant trend that is particularly evident when the content of ZnO is 30%$_{wt}$, *i.e.*, when the dimension of the particles decreases, the PSO model fits the uptake curves better than the PFO. According to the models derivation provided by Azizian,[52] the initial concentration of sorbate (C_0) determines the kinetic regime: PFO adsorption kinetics holds when C_0 is very high compared to the coverage of available sites in the sorbent (θ), while PSO applies when C_0 is not too high with respect to θ. In the case of the ZnCOPs, assuming C_0 as constant in the saturated AcOH

atmosphere, the goodness of PSO *vs.* PFO in fitting the experimental data likely comes from the accessibility of available adsorption sites as the ZnO particles size is changed. Smaller particles produce an overall larger surface area of oxide in contact with the polyurethane network, and thus a larger number of accessible sites available for adsorption of AcOH, which overall is more likely to produce higher coverage. Instead, larger particles expose less surface, which is harder to access by the acid transported through the polymer matrix.

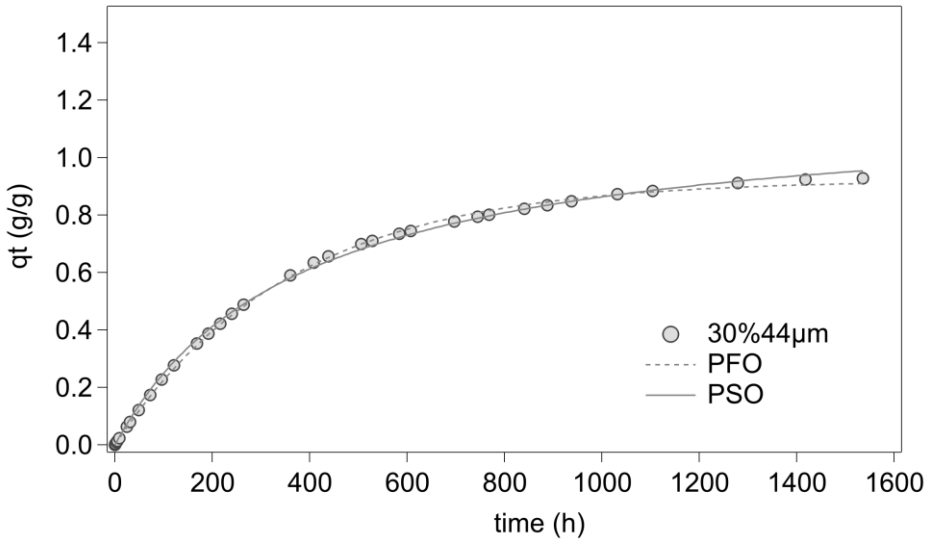

Fig. 5. Adsorption of AcOH by ZnO/COP sample 30%44µm in saturated atmosphere of AcOH at 23°C, fitted to the PFO and PSO models. Errors on the experimental data are included in the markers.

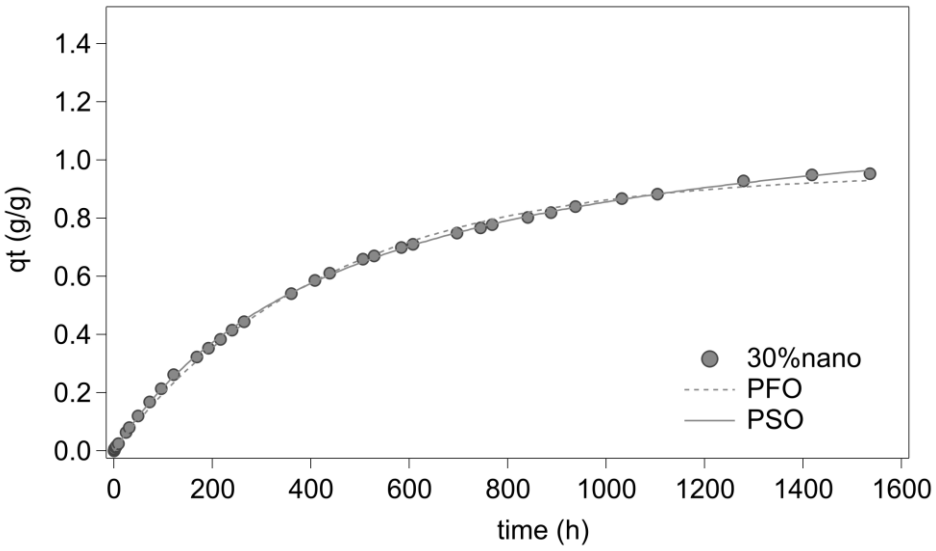

Fig. 6. Adsorption of AcOH by ZnO/COP sample 30%nano in saturated atmosphere of AcOH at 23°C, fitted to the PFO and PSO models. Errors on the experimental data are included in the markers.

When the content of ZnO is reduced to 10%$_{wt}$, the behavior of the ZnO/COP simply approaches that of the COP system, *i.e.*, PSO fits better than PFO for nano- and micron-sized ZnO loaded in the hybrids (see Fig. S13-14 and Annex I in the Supporting Information). The Weibull model provides very good fittings at room temperature, with values of the n_w parameters only slightly larger than 0.75.

When the content of ZnO is increased to 60%$_{wt}$, the PFO and PFO models exhibit worse fittings, with deviations either in the first part or towards the end of the uptake process (see Fig. S15-16), while no satisfactory fittings could be obtained with the IPD or Weibull models. In general, the uptake curves resemble more closely those of the pure ZnO powders (Fig. 4 and Fig. S7-8 in the Supporting Information), as reasonably expected.

3.5 Clustering of the ZnO particles in the Zn/COPs

The morphology of ZnO micro and nanoparticles aggregates in the ZnO/COPs was analyzed to further rationalize the sorption behavior of the materials. In details, the SEM images of ZnO/COP samples 30%44µm, 30%5µm and 30%nano were binarized, as shown in Fig. 7, and analyzed through a MATLAB routine, adapted from Frydendahl *et al*.,[44] that allowed obtaining geometrical descriptors for the systems.

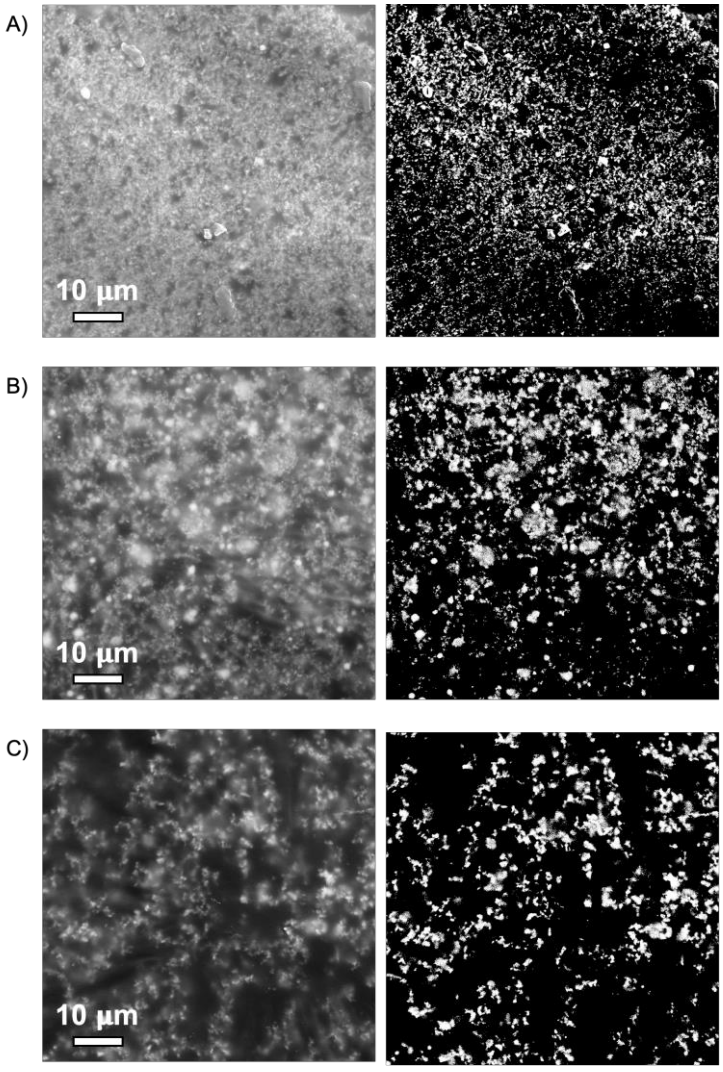

Fig. 7. Some representative SEM images (left) and binarized SEM images (right) of ZnO/COP samples A) 30%nano, B) 30%5µm and C) 30%44µm.

With this approach, each SEM image is associated with a lattice, whose mesh equals the size of a pixel. The aggregates of particles in the binarized images are thus clusters of white pixels, and the perimeters and areas of the clusters can be calculated in pixels. The perimeter *vs.* area relationship for each aggregate, the gyration radius, Rs, the correlation length, ξ, the weighted average of the areas of the clusters, S, and the Hausdorff fractal dimension, D, were calculated for the aggregates observed in the three ZnO/COPs samples. The parameters Rs, ξ and S are all descriptors of the sizes of the clusters detected in the binarized images. The gyration radius, Rs, is defined as the average distance of a site (*i.e.*, a pixel) contained in the cluster, from the center of mass of the cluster:

$$R_s{}^2 = \langle |r_i - r_{cm}|^2 \rangle = \frac{1}{s}\sum_{i=1}^{s} |r_i - r_{cm}|^2 \quad (1)$$

where s is the number of sites in the cluster, r_i is the position of a site in the cluster, and r_{cm} the center of mass, $r_{cm} = \frac{1}{s}\sum_{i=1}^{s} r_i$.

The correlation, or connectivity length, ξ, is the average distance between two sites belonging to the same cluster:

$$\xi^2 = \frac{\sum_s s^2 n_s {R_s}^2}{\sum_s s^2 n_s} \quad (2)$$

Where $n_s = \frac{number\ of\ clusters\ with\ area\ s}{L^2}$ is the cluster number distribution function, with L being the size of the lattice (in pixels), and thus L^2 the total number of sites (pixels); s (number of pixels in a cluster) represents also the area of the cluster.

The weighted average of the areas of the clusters, S, on the other hand, accounts for the number of pixels in a certain cluster, and depends on the cluster number distribution function as well.[67, 68] It is obtained as:

$$S = \frac{\sum_s s^2 n_s}{\sum_s s\, n_s} \quad (3)$$

The Hausdorff fractal dimension, D, describes the clusters roughness. D was calculated using the box counting/scaling method: if a cluster is covered with a grid of a certain mesh-size, the sites of the cluster will occupy N meshes; if the size of cluster is doubled, tripled, *etc.*, while maintaining the shape of the cluster shape, N will change accordingly. A scaling factor, ε, is calculated as the relative variation N undergoes when the area of the cluster increases. Thus, D can be obtained as:

$$D = \frac{\ln(N)}{\ln(\epsilon)} \quad (4)$$

Because the analyzed objects have 2 dimensions, 1<D<2 was expected, and the higher the D values, the higher the roughness.[67]

The previously defined parameters can be compared to get information about the clusters structure and morphology. Log-log plots of the perimeter *vs.* area for the analyzed samples (see Fig. 8A-C) can be fitted to a power law ($y = x^p$), where p is 0.5 for a perfectly circular aggregate (dotted black line reference in the plot panels). The experimental curves for the particles in the ZnO/COPs samples show two different trends: the p value of the smaller aggregates (p1, related to the graph portion closer to the origin) is closer to that of a circle, while larger clusters are more ramified and show more complex architectures (p2 >> 0.5). The p values are listed in Table 2.

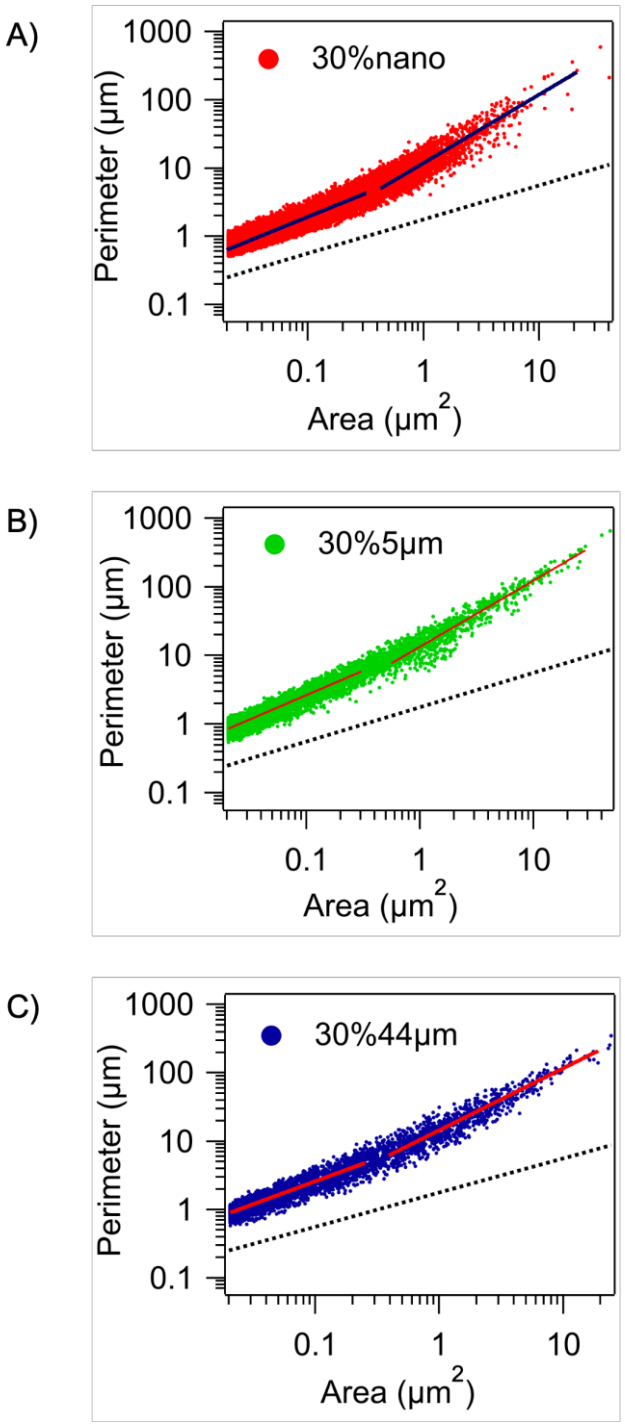

Fig. 8. Perimeter *vs.* area log-log plots for ZnO/COP samples A) 30%nano, b) 30%5µm, and c) 30%44µm, respectively. Fitting lines show the power law relationship ($y = x^p$), which is closer to that of perfectly circular aggregates (black dotted line, p=0.5) for smaller aggregates of particles.

Smaller aggregates are characterized by p1 = 0.67 - 0.71: they are slightly more compact (*i.e.,* spherical) in sample 30%44µm (p1 is closer to that of a perfect circle). Larger aggregates are characterized by p2 = 0.91 – 1.00, with p2 decreasing as the size of the particles increases. The high value of p2 in 30%nano indicates the presence of ramified clusters. Particles in sample 30%5µm have an intermediate behavior, forming objects with protrusions for all the analyzed length scales. Particles in sample 30%44µm, instead, form less complex aggregates.

These observations are also supported by looking at the average ξ and S values (Table 2): the 30%5µm sample has the highest S (largest aggregates with protrusions); ξ, on the other hand, is larger for 30%nano, confirming that the clusters are ramified. ξ decreases as the analyzed objects become more spherical. The large standard deviation on the S values of 30%5µm (Table 2) highlights that the clusters of these particles are more polydisperse than the other systems.

Table 2. Power law fitting results for the perimeter *vs.* area plots (Fig. 8), weighted average cluster area, S, and average correlation length, ξ, of the clusters. Standard deviations were calculated among the values obtained for each analyzed SEM image. Fitting parameters p1 and p2 are the power values obtained for smaller (left portion of the graphs) and larger (right portion of the graphs) clusters, respectively.

Sample name	**Power law fitting results**		**Average S and ξ**	
	p1	**p2**	**S (µm^2)**	**ξ (µm)**
30%nano	0.69 ± 0.01	1.00 ± 0.01	86 ± 44	3.3 ± 1.3
30%5µm	0.71 ± 0.01	0.96 ± 0.01	236 ± 75	2.9 ± 1.1
30%44µm	0.67 ± 0.01	0.91 ± 0.01	142 ± 33	2.8 ± 0.8

Plotting the clusters gyration radius, Rs, *vs.* the number of clusters (Fig. 9A) further confirms some of the previous observations: the three ZnO/COP samples are characterized by a population of small aggregates (with 30%5µm showing the lowest Rs values) and a fraction of large aggregates; the

total number of aggregates detected in the images increases as the size of the particles decreases. The plot of the Hausdorff fractal dimension *vs.* the number of clusters (Fig. 9) indicates that the roughness of the clusters (number of clusters with higher D values) follows the trend 30%44µm > 30%5 µm > 30%nano: larger aggregates of particles are expected to be less homogenous, imparting uneven edges to the 2D shapes detected in the binarized images.

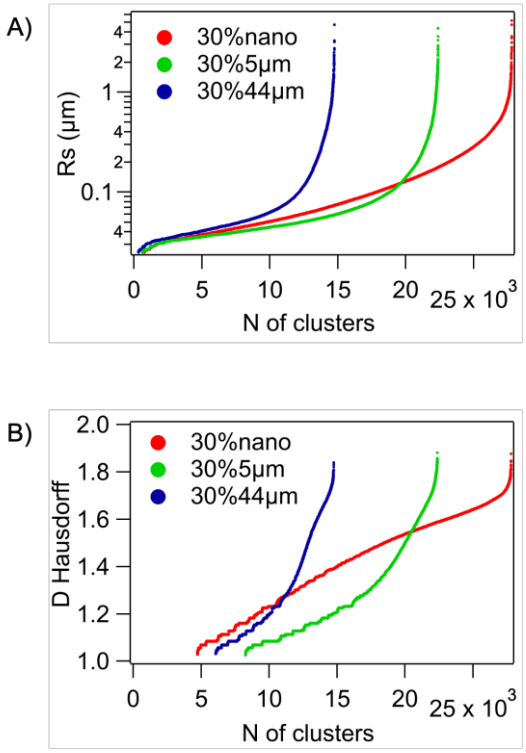

Fig. 9. Plots of the gyration radius, Rs, (A) and of the Hausdorff fractal dimension D (B) *vs.* the number of clusters of ZnO particles for each value, calculated using the binarized SEM images of ZnO/COP samples 30%nano, 30%5µm, and 30%44µm.

To sum up, larger particles (*i.e.*, ZnO particles in 30%44µm Zn/COP sample) form larger aggregates with higher inhomogeneities, *i.e.*, with rougher edges. ZnO particles in sample 30%5µm form polydisperse clusters, with protrusions. Finally, ZnO nanoparticles in sample 30%nano form small, compact, and ramified clusters, with less rough edges.

These observations support the fitting results of the kinetic models in the previous section. Specifically, PFO model fits better the AcOH uptake by the 30%44μm ZnO/COP, *i.e.*, where the particles form the largest aggregates, and thus the ZnO surface area in contact with the hypercrosslinked resin is the smallest. In other words, in these systems AcOH must be transported for longer paths in the resin and can access smaller portions of ZnO, likely resulting in lower coverage of the ZnO surfaces. On the other hand, the nanoparticles in 30%nano form smaller but ramified clusters, with overall larger accessible oxide surface in contact with the resin, which likely produces higher coverage of the ZnO sites by AcOH (better fits with PSO).

3.6 Adsorption kinetics: effect of temperature

As demonstrated in the previous sections, the best kinetic models to fit the experimental data change depending on the content, size and fractality of the ZnO particles included in the COP, and even on the temperature at which exposure to AcOH occurred. PFO and PSO are the only two models that, with some approximation, covered the largest span of possible experimental conditions; thus, they were selected to obtain an evaluation of the activation energies for the overall uptake of acid by the different systems.

The theoretical derivation of PFO and PSO equations as limiting cases from a rigorous Langmuirian model of adsorption model, highlighted the relation of the apparent rate constants used in PFO and PSO (respectively, k_1 and k_2; see also the Supporting Information) with the actual adsorption and desorption rate constants (k_a, k_d) that regulate the adsorption process.[52] In particular, while k_1 has a linear dependence from k_a and k_d weighted by the value of the initial concentration of sorbate ($k_1 = k_aC_0 + k_d$), the k_2 parameter is a much more complex function of C_0, q_e (uptake at the equilibrium), k_a and k_d. Taking into account these considerations, k_1 and k_2 were used in Arrhenius plots (lnk *vs.* 1/T) to evaluate the uptake activation energy values (E_a) for the COP and all the investigated ZnO/COP hybrids. An example (Arrhenius plot for the ZnO/COP system 30%nano) is

shown in Fig. S17. As detailed in the Supporting Information, using the PSO equation in its original scale (y = q(t)) provides a k^*_2 constant, related to the actual k_2 by the simple relation $k^*_2 = k_2 q_e$. In some cases (ZnO/COPs exposed at 45°C) the uptake curves could only be measured for some days, after which the hybrid resins showed degradation; therefore, the theoretical q_e value, obtained from PSO fittings, was used to calculate k_2 from k^*_2. The uptake curves of the pure ZnO powders were fitted up to *ca.* 80% of q(t) values, *i.e.*, before the curves show deviations likely due to disaggregation of the ZnO/zinc acetate grains by extensive sorption. Fitting uptake curves up to 80% of the process (*i.e.*, before equilibrium is reached) is in principle recommended, as kinetics involve processes out of equilibrium.[50] However, in the case of the COP and ZnO/COPs, no relevant differences were noticed when the whole uptake curves were analyzed.

The obtained E_a values are reported in Table 4, where the activated charcoal benchmark is also included as a reference. In all cases, the COP and ZnO/COPs exhibit smaller uptake activation energies than the activated charcoal reference. Moreover, two trends are evident: 1) for the same ZnO content, the activation energy decreases with the size of the particles, *i.e.*, passing from larger to smaller microparticles, and to nanoparticles; 2) for the same type of ZnO particles, the energy decreases when the ZnO content is reduced. In the first case, smaller particles have larger surface area (in contact with the polyurethane network or air), which boosts their reactivity with AcOH. The second trend was instead explained considering that increasing the ZnO content in the resins causes partial aggregation of the particles during the preparation steps, reducing their active surface. The Ea of pure ZnO powders showed higher values compared to those of ZnO/COPs. It was also evident that the smaller the particles, the higher the Ea. Indeed, the smaller the particles, the quicker the reaction of the powder with AcOH and the formation of zinc acetate. The so-formed zinc acetate acts as passive film on the surface of ZnO, contrasting the penetration of AcOH into the bulk powder.

Finally, the enhanced performances of the new absorbers are highlighted considering that the activation energies for the uptake of AcOH either into the pure COP or into the hybrid ZnO/COP gels range ca. between 40 and 50 kJ mol^{-1}. The new COP formulations show thus activation energies for the overall elimination of AcOH that are lower (~ 40% reduction) than those of recent VOC catalysts based solely on inorganic nanostructures, e.g. 77 kJ mol^{-1} for core–shell Al_2O_3@$CoMn_2O_4$ microspheres. The latter have a hollow hierarchical structure supporting Pd nanoparticles, [69] where the elimination mechanism comprises surface adsorption of the VOC on the catalyst surface, the oxidation of the adsorbed intermediates by activated lattice oxygen species, and then re-oxidation by absorbed gas-phase oxygen from air. Other values recently reported for metallic oxide catalysts range between 90 and 175 kJ mol^{-1}. [70] The activation energies for AcOH uptake in the COP gels show also a similar decrease from those needed for the VOC uptake in activated charcoal (~ 78 kJ mol^{-1}). Indeed, even NaOH-impregnated activated carbon filters exhibit adsorption capacities of AcOH of only 0.5-0.6 g/g, [66] whereas the hybrid ZnO/COPs range around 0.9-1.0 g/g. The hybrid gels perform also much better than recently reported ion-exchange resins with tertiary or quaternary amino functional groups on a styrene–divinyl benzene copolymer matrix, which have capacities ranging from ca. 0.2 to 0.6 g/g, [71] where uptake was described in terms of adsorption reinforced by specific acid interaction with the resin functional groups.

Overall, these comparisons indicate that the presence of an uptake mechanism with two synergistic steps (transport in the COP matrix and adsorption at the particles' surface) is likely key to yield enhanced VOC removal with respect to state-of-the-art systems where VOC uptake is mostly based on surface adsorption.

Table 3. Activation energy (E_a) values calculated from Arrhenius plots for the AcOH uptake by COP and Zn/COP samples, and the activated charcoal reference, fitted to the PFO and PSO kinetic

models. The reported R^2 values refer to the plots obtained using the apparent rate constants k_1 (PFO) and k_2 (PSO).

Sample name	**PFO**		**PSO**	
	E_a (kJ mol^{-1})	**R^2**	**E_a (kJ mol^{-1})**	**R^2**
COP	47.7±13.8	0.856	42.4±13.8	0.825
10%nano	38.2±8.6	0.907	27.8±7.5	0.874
30%nano	40.2±4.4	0.976	37.0±2.7	0.989
60%nano	53.9±16.5	0.842	57.5±11.4	0.927
10%5µm	42.9±10.8	0.887	36.7±9.8	0.874
30%5µm	41.8±2.2	0.994	34.9±12.5	0.796
60%5µm	54.0±12.1	0.908	66.6±11.0	0.948
10%44µm	43.5±10.0	0.904	36.9±13.7	0.785
30%44µm	45.3±13.4	0.851	38.3±11.2	0.855
60%44µm	62.2±2.9	0.996	72.7±10.6	0.959
ZnO-nano	147.7±10.3	0.990	162.8±13.1	0.987
ZnO-5µm	120.6±33.8	0.707	154.0±42.7	0.867
ZnO-44µm	116.6±12.1	0.979	137.9±12.0	0.985
Ac. charcoal	78.3±4.2	0.994	93.6±2.1	0.999

Table 4. Summary of the advantages of the new ZnO/COPs hybrids demonstrated in this contribution, as compared to state-of-the-art materials for the removal of VOCs. The key features are the hybrids' lower overall activation energy for the removal process, high uptake capacity, and lack of critical limitations in the handling, use and safety.

VOCs removal activation energy		
Material	**Ea (kJ mol^{-1})**	**Ref.**
Pd/$CoMn_2O_4$ supported on Al_2O_3	77	[69]
Mn-Cu	90-175	[70]
NaOH impregnated AC	78	[66]
ZnO/COPs hybrids	40-50	This work

AcOH uptake capacity in gas phase			
Material	**Adsorption capacity (g AcOH/ g sample)**	**Drawbacks**	**Ref.**
Carbon	0.44-0.54	Low adsorption capacity, desorption of VOCs, powdery form (lacks safety to users and artifacts)	[21]
Zeolite 13X, BDH	1.25	Powdery form	[21]
Comm. available Zeolite Y	0.48	Low adsorption capacity, powdery form	[21]
Pillared clay	0.28	Low adsorption capacity, powdery form (lacks safety to users and artifacts)	[21]
Silica gel 60	0.07	Very low adsorption capacity, powdery form (lacks safety to users and artifacts)	[21]
NaOH impregnated AC	0.5-0.6	Low adsorption capacity, powdery form	[21]
ZnO/COPs hybrids	0.85-1.15	- (No major handling/safety issues)	This work

4. Conclusions

Starting from the formulation of hybrid zinc oxide-castor oil polyurethane resins (ZnO/COPs) previously reported,[7] it was demonstrated here how the enhanced removal of acetic acid (AcOH) by the hybrids can be obtained playing on the size, content and fractality of the ZnO particles embedded in the COP resins. Controlling these factors affect the kinetics of AcOH uptake in the resins, allowing for formulations whose properties surpass state-of-the-art systems for VOC removal in different fields, including the preventive conservation of masterpieces in museums and exhibitions. In fact, while research is growingly considering synthetic and bio-polymers to formulate hydro- and organogels for cleaning artifacts,[8-12] the use of functional hybrid polymer networks and colloidal particles in preventive art conservation is still vastly unexplored. Moreover,

traditional and state-of-the-art absorbers all exhibit drawbacks related to manufacturing costs, scarce retention of captured VOCs, or safety/environmental issues.[20-25]

The starting hypothesis was that the COP network would act as a transporter of AcOH via the formation and rupture of weak interactions, while adsorption was expected to dominate the interaction of the acid with the surface of the ZnO micro or nanoparticles. Such mechanism was demonstrated here by fitting the experimental curves of AcOH uptake in the COP and hybrid networks at different temperatures. Either pseudo first order (PFO) or pseudo second order (PSO) models provided the best fitting for the kinetics of the ZnO/COPs, and the collected data suggest dependence on the different coverage of the ZnO surface by AcOH in the case of micron- or nano-sized oxide particles. These findings provide experimental evidence that supports the theoretical derivation of these kinetic models from the classical Langmuirian adsorption model.[41] This conclusion was corroborated by the analysis of morphology and fractal dimension of the ZnO particles in the hybrid networks: micron-sized particles form lager clusters, while nanoparticles form smaller but ramified clusters that are more likely to be accessed and covered by adsorbed AcOH. Decreasing the size of the particles from microns to nanometers reduces the activation energy of the process, boosting the VOC removal efficiency.

The two-steps uptake mechanism that was showed here for the first time for the ZnO/COPs hybrids (diffusion and Case-II transport in the polymer matrix and adsorption at the particles surface) is key to produce the enhanced removal of AcOH by this new class of absorbers, which candidate as new promising tools for pollution remediation. The higher performances of the new hybrids versus state-of-the-art and traditional materials (metal and metallic oxide nanoparticles, activated carbons, zeolites) have been summarized in Table 4, showing the advantages of the ZnO/COPs in terms of reduced activation energy for the overall VOC removal, AcOH uptake capacity, and safety/practical considerations. Thanks to these advantages, the new absorbers have been positively tested for application in museum and other indoor environments.[72] Further study will expand the

possibilities of these new absorbers when different classes of inorganic colloidal particles are uploaded in the COP matrix, or when the matrix is functionalized (e.g. using different cross-linkers).

Overall, the ZnO/COPs hybrids candidate as highly promising tools not only in the preventive conservation of masterpieces in museums/exhibition/deposits, but also in other fields where efficient capture of acetic acid is crucial and currently lacking (food industry, textile dyeing/printing, *etc*.).

CRediT authorship contribution statement

Alessio Zuliani: Conceptualization; Data acquisition and analysis; Investigation; Methodology; Writing. **David Chelazzi**: Conceptualization; Data acquisition and analysis; Methodology; Writing. **Rosangela Mastrangelo:** Data acquisition and analysis; Investigation; Methodology; Writing. **Rodorico Giorgi**: Conceptualization; Data acquisition and analysis; Methodology; Writing. **Piero Baglioni**: Supervision; Conceptualization; Validation; Data analysis; Funding acquisition; Methodology; Project administration; Writing.

Declaration of Competing Interest

The authors declare that they have no known competing financial interests or personal relationships that could have appeared to influence the work reported in this paper.

Acknowledgements

This project has received funding from the European Union's Horizon 2020 research and innovation programme under grant agreement Nº814496. This publication reflects only the author's

view, exempting the European Union from any liability. Project website: https://www.apacheproject.eu/.

Supporting Information

Complete Raman spectroscopy analysis; description of the kinetic models; additional adsorption curves; Arrhenius plot for the AcOH uptake by sample 30%nano, fitted to the PFO and PSO kinetic models; Annex I: complete list of the fitting parameters and errors of all the adsorption curves.

References

[1] D. Chelazzi, G. Poggi, Y. Jaidar, N. Toccafondi, R. Giorgi, P. Baglioni, Hydroxide nanoparticles for cultural heritage: Consolidation and protection of wall paintings and carbonate materials, Journal of Colloid and Interface Science 392 (2013) 42-49. DOI: 10.1016/j.jcis.2012.09.069.

[2] P. Baglioni, E. Carretti, D. Chelazzi, Nanomaterials in art conservation, Nature Nanotechnology 10(4) (2015) 287-290. DOI: 10.1038/nnano.2015.38.

[3] P. Baglioni, D. Chelazzi, How Science Can Contribute to the Remedial Conservation of Cultural Heritage, Chemistry-a European Journal 27(42) (2021) 10798-10806. DOI: 10.1002/chem.202100675.

[4] T. Fistos, I. Fierascu, R.C. Fierascu, Recent Developments in the Application of Inorganic Nanomaterials and Nanosystems for the Protection of Cultural Heritage Organic Artifacts, Nanomaterials 12(2) (2022). DOI: 10.3390/nano12020207.

[5] R. Mastrangelo, D. Chelazzi, G. Poggi, E. Fratini, L.P. Buemi, M.L. Petruzzellis, P. Baglioni, Twin-chain polymer hydrogels based on poly(vinyl alcohol) as new advanced tool for the cleaning of modern and contemporary art, Proceedings of the National Academy of Sciences of the United States of America 117(13) (2020) 7011-7020. DOI: 10.1073/pnas.1911811117.

[6] K. Dedecker, R.S. Pilla, F. Nouar, J. Pires, N. Steunou, E. Dumas, G. Maurin, C. Serre, M.L. Pinto, Metal-Organic Frameworks for Cultural Heritage Preservation: The Case of Acetic Acid Removal, Acs Applied Materials & Interfaces 10(16) (2018) 13886-13894. DOI: 10.1021/acsami.8b02930.

[7] A. Zuliani, D. Bandelli, D. Chelazzi, R. Giorgi, P. Baglioni, Environmentally friendly ZnO/Castor oil polyurethane composites for the gas-phase adsorption of acetic acid, Journal of Colloid and Interface Science 614 (2022) 451-459. DOI: 10.1016/j.jcis.2022.01.123.

[8] P. Baglioni, N. Bonelli, D. Chelazzi, A. Chevalier, L.G. Dei, J. Domingues, E. Fratini, R. Giorgi, M. Martin, Organogel formulations for the cleaning of easel paintings, Applied Physics a-Materials Science & Processing 121(3) (2015) 857-868. DOI: 10.1007/s00339-015-9364-0.

[9] N. Bonelli, C. Montis, A. Mirabile, D. Berti, P. Baglioni, Restoration of paper artworks with microemulsions confined in hydrogels for safe and efficient removal of adhesive tapes, Proceedings of the National Academy of Sciences of the United States of America 115(23) (2018) 5932-5937. DOI: 10.1073/pnas.1801962115.

[10] M. Baglioni, J.A.L. Domingues, E. Carretti, E. Fratini, D. Chelazzi, R. Giorgi, P. Baglioni, Complex Fluids Confined into Semi-interpenetrated Chemical Hydrogels for the Cleaning of Classic Art: A Rheological and SAXS Study, Acs Applied Materials & Interfaces 10(22) (2018) 19162-19172. DOI: 10.1021/acsami.8b01841.

[11] V. Rosciardi, D. Chelazzi, P. Baglioni, "Green" biocomposite Poly (vinyl alcohol)/starch cryogels as new advanced tools for the cleaning of artifacts, Journal of Colloid and Interface Science 613 (2022) 697-708. DOI: 10.1016/j.jcis.2021.12.145.

[12] T. Guaragnone, M. Rossi, D. Chelazzi, R. Mastrangelo, M. Severi, E. Fratini, P. Baglioni, pH-Responsive Semi-Interpenetrated Polymer Networks of pHEMA/PAA for the Capture of Copper Ions and Corrosion Removal, ACS Applied Materials & Interfaces 14(5) (2022) 7471-7485. DOI: 10.1021/acsami.1c22837.

[13] K. Martina, F. Calsolaro, A. Zuliani, G. Berlier, F. Chavez-Rivas, M.J. Moran, R. Luque, G. Cravotto, Sonochemically-Promoted Preparation of Silica-Anchored Cyclodextrin Derivatives for Efficient Copper Catalysis, Molecules 24(13) (2019). DOI: 10.3390/molecules24132490.

[14] C.M. Cova, A. Zuliani, M.J. Munoz-Batista, R. Luque, Efficient Ru-based scrap waste automotive converter catalysts for the continuous-flow selective hydrogenation of cinnamaldehyde, Green Chemistry 21(17) (2019) 4712-4722. DOI: 10.1039/c9gc01596e.

[15] A. Zuliani, C.M. Cova, R. Manno, V. Sebastian, A.A. Romero, R. Luque, Continuous flow synthesis of menthol *via* tandem cyclisation-hydrogenation of citronellal catalysed by scrap catalytic converters, Green Chemistry 22(2) (2020) 379-387. DOI: 10.1039/c9gc03299a.

[16] C.M. Cova, A. Zuliani, R. Manno, V. Sebastian, R. Luque, Scrap waste automotive converters as efficient catalysts for the continuous-flow hydrogenations of biomass derived chemicals, Green Chemistry 22(4) (2020) 1414-1423. DOI: 10.1039/c9gc04091a.

[17] A. Zuliani, C.M. Cova, Green Synthesis of Heterogeneous Visible-Light-Active Photocatalysts: Recent Advances, Photochem 1(2) (2021) 147-166. DOI: 10.3390/photochem1020009

[18] A. Zuliani, M. Cano, F. Calsolaro, A.R. Puente Santiago, J.J. Giner-Casares, E. Rodríguez-Castellón, G. Berlier, G. Cravotto, K. Martina, R. Luque, Improving the electrocatalytic performance of sustainable Co/carbon materials for the oxygen evolution reaction by ultrasound and microwave assisted synthesis, Sustainable Energy & Fuels 5(3) (2021) 720-731. DOI: 10.1039/D0SE01505A.

[19] A. Zuliani, O. Kikhtyanin, C. M. Cova, D. Rodriguez-Padron, D. Kubička, R. Luque, Boosting the Ni-Catalyzed Hydrodeoxygenation (HDO) of Anisole Using Scrap Catalytic Converters, Advanced Sustainable Systems 6 (2022) 2100394. DOI: 10.1002/adsu.202100394.

[20] J. Ren, X. Dyosiba, N. M. Musyoka, H. W. Langmi, M. Mathe, S. Liao, Review on the current practices and efforts towards pilot-scale production of metal-organic frameworks (MOFs), Coordination Chemistry Reviews 352 (2017) 187-219. DOI: 10.1016/j.ccr.2017.09.005.

[21] J. Pires, A.C. Araújo, A.P. Carvalho, M.L. Pinto, J.M. González-Calbet, J. Ramírez-Castellanos, Porous materials from clays by the gallery template approach: synthesis, characterization and adsorption properties, Microporous and Mesoporous Materials 73(3) (2004) 175-180. DOI: 10.1016/j.micromeso.2004.05.009.

[22] X. Zhang, B. Gao, A. E. Creamer, C. Cao, Y. Li, Adsorption of VOCs onto engineered carbon materials: A review, Journal of Hazardous Materials 338 (2017) 102-123. DOI: 10.1016/j.jhazmat.2017.05.013.

[23] A. João Cruz, J. Pires, A. P. Carvalho, M. Brotas de Carvalho, Adsorption of acetic acid by activated carbons, zeolites, and other adsorbent materials related with the preventive conservation of lead objects in museum showcases, Journal of Chemical & Engineering Data 49(3) (2004) 725-731. DOI: 10.1021/je034273w.

[24] https://eur-lex.europa.eu/legal-content/EN/ALL/?uri=celex%3A52008DC0397 "Communication from the Commission to the European Parliament, the Council, the European Economic and Social Committee and the Committee of the Regions on the Sustainable Consumption and Production and Sustainable Industrial Policy Action Plan {SEC(2008) 2110} {SEC(2008) 2111}" accessed in September 2022.

[25] S. Wang, L. Zhang, C. Long, A. Li, Enhanced adsorption and desorption of VOCs vapor on novel micro-mesoporous polymeric adsorbents, Journal of Colloid and Interface Science 428 (2014) 185-190. DOI: 10.1016/j.jcis.2014.04.055.

[26] J. Huang, S.R. Turner, Hypercrosslinked Polymers: A Review, Polymer Reviews 58(1) (2018) 1-41. DOI: 10.1080/15583724.2017.1344703.

[27] K. Wang, W.W. Cui, Z.Y. Bian, Y.Q. Liu, S. Jiang, Y. Zhou, J. Wang, Size and stability modulation of Pd nanoparticles on porous hypercrosslinked ionic polymer for heterogeneous aerobic oxidative coupling of diaryl ether, Applied Catalysis B-Environmental 281 (2021). DOI: 10.1016/j.apcatb.2020.119425.

[28] Y. Cheng, S. Razzaque, Z. Zhan, B.E. Tan, Construction and gas uptake performance of cyano-functional hypercrosslinked polymers via knitting strategy, Chemical Engineering Journal 426 (2021). DOI: 10.1016/j.cej.2021.130731.

[29] J.H. Huang, X.Y. Jin, J.L. Mao, B. Yuan, R.J. Deng, S.G. Deng, Synthesis, characterization and adsorption properties of diethylenetriamine-modified hypercrosslinked resins for efficient removal of salicylic acid from aqueous solution, Journal of Hazardous Materials 217 (2012) 406-415. DOI: 10.1016/j.jhazmat.2012.03.053.

[30] J.H. Huang, X.Y. Jin, S.G. Deng, Phenol adsorption on an N-methylacetamide-modified hypercrosslinked resin from aqueous solutions, Chemical Engineering Journal 192 (2012) 192-200. DOI: 10.1016/j.cej.2012.03.078.

[31] J.H. Huang, B. Yuan, X.F. Wu, S.G. Deng, A comparative adsorption study of beta-naphthol on four polymeric adsorbents from aqueous solutions, Journal of Colloid and Interface Science 380 (2012) 166-172. DOI: 10.1016/j.jcis.2012.05.022.

[32] X.M. Wang, X.J. Yuan, S. Han, H.W. Zha, X.C. Sun, J.H. Huang, Y.N. Liu, Aniline modified hypercrosslinked polystyrene resins and their adsorption equilibriums, kinetics and dynamics towards salicylic acid from aqueous solutions, Chemical Engineering Journal 233 (2013) 124-131. DOI: 10.1016/j.cej.2013.08.039.

[33] X.T. Li, Y.F. Liu, D.L. Di, G.H. Wang, Y. Liu, A formaldehyde carbonyl groups-modified self-crosslinked-polystyrene resin: Synthesis, adsorption and separation properties, Colloids and Surfaces a-Physicochemical and Engineering Aspects 500 (2016) 1-9. DOI: 10.1016/j.colsurfa.2016.03.061.

[34] T.J. Robshaw, A.M. James, D.B. Hammond, J. Reynolds, R. Dawson, M.D. Ogden, Calcium-loaded hydrophilic hypercrosslinked polymers for extremely high defluoridation capacity via multiple uptake mechanisms, Journal of Materials Chemistry A 8(15) (2020) 7130-7144. DOI: 10.1039/c9ta12285k.

[35] Y. Sun, Y.P. Gu, J.P. Yang, Adsorption of N-heterocyclic compounds from aqueous solutions by sulfonic acid-functionalized hypercrosslinked resins in batch experiments, Chemical Engineering Journal 428 (2022). DOI: 10.1016/j.cej.2021.131163.

[36] C. Long, Y. Li, W.H. Yu, A.M. Li, Removal of benzene and methyl ethyl ketone vapor: Comparison of hypercrosslinked polymeric adsorbent with activated carbon, Journal of Hazardous Materials 203 (2012) 251-256. DOI: 10.1016/j.jhazmat.2011.12.010.

[37] S.S. Wang, L. Zhang, C. Long, A.M. Li, Enhanced adsorption and desorption of VOCs vapor on novel micro-mesoporous polymeric adsorbents, Journal of Colloid and Interface Science 428 (2014) 185-190. DOI: 10.1016/j.jcis.2014.04.055.

[38] L.J. Jia, W.H. Yu, C. Long, A.M. Li, Adsorption equilibrium and dynamics of gasoline vapors onto polymeric adsorbents, Environmental Science and Pollution Research 21(5) (2014) 3756-3763. DOI: 10.1007/s11356-013-2328-z.

[39] L.Y. Wu, L.J. Jia, X.H. Liu, C. Long, The prediction of adsorption isotherms of ester vapors on hypercrosslinked polymeric adsorbent, Frontiers of Environmental Science & Engineering 10(3) (2016) 482-490. DOI: 10.1007/s11783-015-0826-6.

[40] J. Wu, L.J. Jia, L.Y. Wu, C. Long, W.B. Deng, Q.X. Zhang, Prediction of the breakthrough curves of VOC isothermal adsorption on hypercrosslinked polymeric adsorbents in a fixed bed, Rsc Advances 6(34) (2016) 28986-28993. DOI: 10.1039/c6ra01310d.

[41] L.J. Jia, J.K. Ma, Q.Y. Shi, C. Long, Prediction of Adsorption Equilibrium of VOCs onto Hyper-Cross-Linked Polymeric Resin at Environmentally Relevant Temperatures and Concentrations Using Inverse Gas Chromatography, Environmental Science & Technology 51(1) (2017) 522-530. DOI: 10.1021/acs.est.6b05039.

[42] L. Ernstgard, A. Iregren, B. Sjogren, G. Johanson, Acute effects of exposure to vapours of acetic acid in humans, Toxicology Letters 165(1) (2006) 22-30. DOI: 10.1016/j.toxlet.2006.01.010.

[43] C.M. Cova, E. Rincón, E. Espinosa, L. Serrano, A. Zuliani, Paving the Way for a Green Transition in the Design of Sensors and Biosensors for the Detection of Volatile Organic Compounds (VOCs), Biosensors 12(2) (2022). DOI: 10.3390/bios12020051.

[44] Fractal analysis package version 1.0.2 (175 KB) by Christian Frydendahl. Available online: https://www.mathworks.com/matlabcentral/fileexchange/71770-fractal-analysis-package (accessed on April 2022).

[45] M. Rajalakshmi, A.K. Arora, B.S. Bendre, S. Mahamuni, Optical phonon confinement in zinc oxide nanoparticles, Journal of Applied Physics 87(5) (2000) 2445-2448. DOI: 10.1016/j.heliyon.2019.e01222.

[46] V.I. Korepanov, S.Y. Chan, H.C. Hsu, H.O. Hamaguchi, Phonon confinement and size effect in Raman spectra of ZnO nanoparticles, Heliyon 5(2) (2019). DOI: 10.1063/1.372199.

[47] T. Ishioka, Y. Shibata, M. Takahashi, I. Kanesaka, Y. Kitagawa, K.T. Nakamura, Vibrational spectra and structures of zinc carboxylates I. Zinc acetate dihydrate, Spectrochimica Acta Part a-Molecular and Biomolecular Spectroscopy 54(12) (1998) 1827-1835. DOI: 10.1016/s1386-1425(98)00063-8.

[48] N.L. Parada Hernandez, A.J. Bonon, J.O. Bahú, M.I.R. Barbosa, M.R. Wolf Maciel, R.M. Filho, Epoxy monomers obtained from castor oil using a toxicity-free catalytic system, J Mol Catal A Chem. 426 (2017) 550–556. DOI: 10.1016/J.MOLCATA.2016.08.005.

[49] F.O.V. da Cunha, D.H.R. Melo, V.B. Veronese, M.M.C. Forte, Study of castor oil polyurethane - poly(methyl methacrylate) semi-interpenetrating polymer network (SIPN) reaction parameters using a 2^3 factorial experimental design, Materials Research. 7 (2004) 539–543. DOI: 10.1590/S1516-14392004000400006.

[50] S. Parnell, K. Min, M. Cakmak, Kinetic studies of polyurethane polymerization with Raman spectroscopy, Polymer (Guildf). 44 (2003) 5137–5144. DOI: 10.1016/S0032-3861(03)00468-3.

[51] M.K. Johnson, D.B. Powell, R.D. Cannon, Vibrational spectra of carboxylato complexes—I. Infrared and Raman spectra of beryllium(II) acetate and formate and of zinc(II) acetate and zinc(II) acetate dihydrate, Spectrochim Acta A. 37 (1981) 899–904. DOI: 10.1016/0584-8539(81)80011-6.

[52] S. Azizian, Kinetic models of sorption: a theoretical analysis, Journal of Colloid and Interface Science 276(1) (2004) 47-52. DOI: 10.1016/j.jcis.2004.03.048.

[53] W. Plazinski, W. Rudzinski, A. Plazinska, Theoretical models of sorption kinetics including a surface reaction mechanism: A review, Advances in Colloid and Interface Science 152(1-2) (2009) 2-13. DOI: 10.1016/j.cis.2009.07.009.

[54] J.P. Simonin, On the comparison of pseudo-first order and pseudo-second order rate laws in the modeling of adsorption kinetics, Chemical Engineering Journal 300 (2016) 254-263. DOI: 10.1016/j.cej.2016.04.079.

[55] O. Baytar, O. Sahin, S. Horoz, S. Kutluay, High-performance gas-phase adsorption of benzene and toluene on activated carbon: response surface optimization, reusability, equilibrium, kinetic, and competitive adsorption studies, Environmental Science and Pollution Research 27(21) (2020) 26191-26210. DOI: 10.1007/s11356-020-08848-4.

[56] G.E. Boyd, A.W. Adamson, L.S. Myers, The Exchange Adsorption of Ions from Aqueous Solutions by Organic Zeolites. II. Kinetics1, Journal of the American Chemical Society 69(11) (1947) 2836-2848. DOI: 10.1021/ja01203a066.

[57] J. Weber Walter, J.C. Morris, Kinetics of Adsorption on Carbon from Solution, Journal of the Sanitary Engineering Division 89(2) (1963) 31-59. DOI: 10.1061/JSEDAI.0000430 (acccessed 2022/03/14).

[58] J.P. Simonin, J. Boute, Intraparticle diffusion-adsorption model to describe liquid/solid adsorption kinetics, Revista Mexicana De Ingenieria Quimica 15(1) (2016) 161-173.

[59] V. Russo, R. Tesser, D. Masiello, M. Trifuoggi, M. Di Serio, Further verification of adsorption dynamic intraparticle model (ADIM) for fluid-solid adsorption kinetics in batch reactors, Chemical Engineering Journal 283 (2016) 1197-1202. DOI: 10.1016/j.cej.2015.08.066.

[60] N. Chiron, R. Guilet, E. Deydier, Adsorption of Cu(II) and Pb(II) onto a grafted silica: isotherms and kinetic models, Water Research 37(13) (2003) 3079-3086. DOI: 10.1016/s0043-1354(03)00156-8.

[61] T.A. Metts, S.A. Batterman, Effect of VOC loading on the ozone removal efficiency of activated carbon filters, Chemosphere 62(1) (2006) 34-44. DOI: 10.1016/j.chemosphere.2005.04.049.

[62] F.C. Wu, R.L. Tseng, R.S. Juang, Characteristics of Elovich equation used for the analysis of adsorption kinetics in dye-chitosan systems, Chemical Engineering Journal 150(2-3) (2009) 366-373. DOI: 10.1016/j.cej.2009.01.014.

[63] V. Papadopoulou, K. Kosmidis, M. Vlachou, P. Macheras, On the use of the Weibull function for the discernment of drug release mechanisms, International Journal of Pharmaceutics 309(1-2) (2006) 44-50. DOI: 10.1016/j.ijpharm.2005.10.044.

[64] B. Subramanyam, A. Das, Linearised and non-linearised isotherm models optimization analysis by error functions and statistical means, Journal of Environmental Health Science and Engineering 12 (2014). DOI: 10.1186/2052-336x-12-92.

[65] S. Shahmohammadi-Kalalagh, H. Babazadeh, Isotherms for the sorption of zinc and copper onto kaolinite: comparison of various error functions, International Journal of Environmental Science and Technology 11(1) (2014) 111-118. DOI: 10.1007/s13762-013-0260-x.

[66] S. Wang, H. Nam, T.B. Gebreegziabher, Adsorption of acetic acid and hydrogen sulfide using NaOH impregnated activated carbon for indoor air purification, Engineering Reports 2(1) (2020). DOI: 10.1002/eng2.12083.

[67] D. Stauffer, A. Aharony, Introduction to percolation theory: second edition., 2nd edition ed., Taylor & Francis1992. DOI: 10.1201/9781315274386.

[68] C. Frydendahl, M. Grajower, J. Bar-David, R. Zektzer, N. Mazurski, J. Shappir, U. Levy, Giant enhancement silicon plasmonic shortwave infrared photodetection using nanoscale self-organized metallic films, Optica 7(5) (2020) 371-379. DOI: 10.1364/optica.379549.

[69] J. He, F. Zheng, Y. Zhou, X. Li, Y. Wang, J. Xiao, Y. Li, D. Chen, J. Lu, Catalytic oxidation of VOCs over 3D@2D Pd/$CoMn_2O_4$ nanosheets supported on hollow Al_2O_3 microspheres, Journal of Colloid and Interface Science 613 (2022) 155-167. DOI: 10.1016/j.jcis.2022.01.023.

[70] J. R. Li, W. P. Zhang, C. Li, C. He, Efficient catalytic degradation of toluene at a readily prepared Mn-Cu catalyst: Catalytic performance and reaction pathway, Journal of Colloid and Interface Science 591 (2021) 396-408. DOI: 10.1016/j.jcis.2021.01.096.

[71] H.M Anasthas, V.G Gaikar, Adsorption of acetic acid on ion-exchange resins in non-aqueous conditions, Reactive and Functional Polymers 47(1) (2001) 23-35. DOI: 10.1016/S1381-5148(00)00066-3.

[72] P. Baglioni, D. Chelazzi, A. Zuliani, R. Giorgi, VOC adsorbing component made of castor oil-based organic-inorganic composite material". Patent PO022467IT priority June 3 2021 and PCT/EP2022/060963, priority April 26 2022.

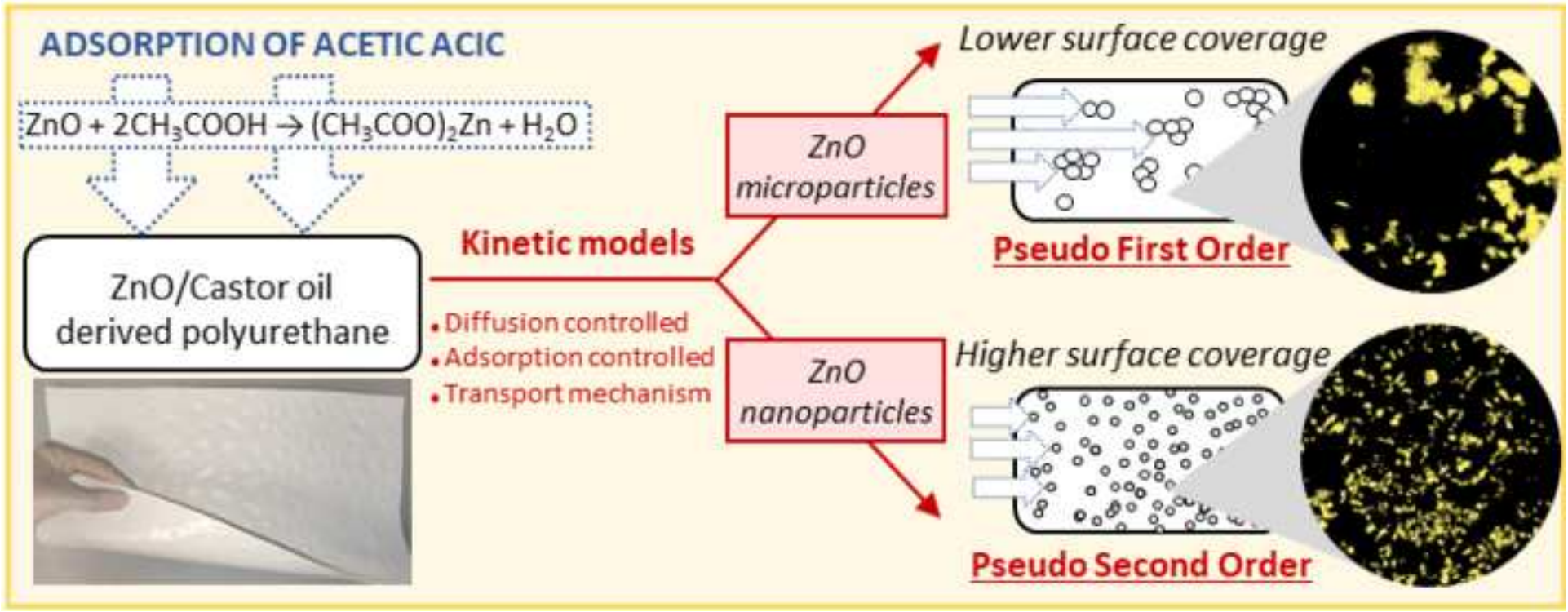

Credit authorship contribution statement

Alessio Zuliani: Conceptualization; Data acquisition and analysis; Investigation; Methodology; Writing. **David Chelazzi**: Conceptualization; Data acquisition and analysis; Methodology; Writing. **Rosangela Mastrangelo:** Data acquisition and analysis; Investigation; Methodology; Writing. **Rodorico Giorgi**: Conceptualization; Data acquisition and analysis; Methodology; Writing. **Piero Baglioni**: Supervision; Conceptualization; Validation; Data analysis; Funding acquisition; Methodology; Project administration; Writing.